Progress In Electromagnetics Research M, Vol. 32, 181–200, 2013

DESIGN OF SPIRAL CIRCULAR COILS IN WET AND DRY TISSUE FOR BIO-IMPLANTED MICRO-SYSTEM APPLICATIONS

Saad Mutashar[1, 2, *], M. A. Hannan[1], Salina A. Samad[1], and Aini Hussain[1]

[1]Department of Electrical, Electronic & Systems Engineering, Faculty of Engineering and Built Environment, Universiti Kebangsaan Malaysia, UKM, Bangi, Selangor 43600, Malaysia

[2]Department of Electrical and Electronic Engineering, University of Technology, Baghdad, Iraq

Abstract—This paper deals with the design of small-sized bio-implanted spiral circular coils (pancake) with an operating frequency of 13.56 MHz. The external and internal coils' geometric dimensions are $d_{out} = 56$ mm, $d_{in} = 10$ mm and $d_{out} = 11.6$ mm, $d_{in} = 5$ mm, respectively, in which the electrical performance is verified through the commercial field solver High Frequency Structural Simulator (HFSS 13.0), which employs the finite-element method (FEM) technique. Mathematical models for the proposed coils are developed. The simulation is performed-based on the developmental model in the air and at depths 6 mm in a human biological tissue of dry and wet skin. The results demonstrate that the external and internal coils have maximum near-field gains of 54.15 dB and 53.30 dB in air. The maximum gains of the external coil contacted the wet and dry skin are 49.80 dB and 48.95 dB, respectively. The maximum gains of the internal coil at depths of 6 mm in the wet and dry tissue are 41.80 dB and 41.40 dB, respectively. However, the external coil radiation efficiencies on wet- and dry-skin are 92% and 90%, respectively, compared with that on air. The internal coil radiation efficiencies on wet- and dry-skin are 78.4% and 77.6%, respectively, compared with that on air. In this study, the specific absorption rate (SAR) and radiated power results of the internal coil are investigated using SEMCAD 16.4 software. The SAR and power loss studies show that the designed implanted coil has a negligible effect on the wet and dry skin and can be ignored.

Received 27 May 2013, Accepted 29 July 2013, Scheduled 21 August 2013

* Corresponding author: Saad Mutashar (saad_ra25@yahoo.com).

1. INTRODUCTION

In the last decade, the wireless power transfer (WPT) plays an important role in many applications and is widely used in near-field inductive coupling links. Currently, most of the implanted devices are powered inductively such as implanted cochlear, retinal implants and implanted micro-systems, used to stimulate and monitoring nerves and muscle activities [1–4]. The power efficiency of the inductive coupling links of the implanted devices is affected by power loss in the electric circuits of the devices and energy absorption by the biological tissues. The electric circuits involve two parts: the external and internal parts. The external part located outside the body can be accurate with flexibility in the design in terms of size, especially the size of the transmitter coil. While the internal part is located within the human body and should be carefully designed to the smallest possible size, especially the receiver coil, to maximize the patients' comfort. The medium separating the coils in each of the parts is biological tissue [5].

The penetration of the electromagnetic (EM) waves will occur inside the biological tissues, such as skins, fat and muscles, to achieve an inductive connection link with the implanted part [6]. The tissue temperature will be increased due to the transmission of the signal through it. Hence, the energy of EM signals, absorbed by tissue, may damage the tissue. To avoid this, the operated frequency of the system should be considered carefully [7]. However, the human body consists of about 65%–70% of water. Therefore, the industrial specific medical (ISM) assigned the low frequency band to transmit power and data through the human body and should be lower than 20 MHz such as frequencies (125–134 kHz, 6.78 MHz and 13.56 MHz) which did not lose much of their energy through water, hence, not damage the tissue [8].

To disregard the EM effects on the human biological tissues and the expected amount of the absorption of energy in the tissue, the relative permittivity, conductivity and loss of tangent of air is designed in such a way that air is placed between the inductive links. In contrast, the constitutive parameters of the tissues vary depending on the different frequency changes. The constitutive parameters of air and human biological tissue are different; hence, designers should consider the tissue as a medium between coils. Many studies have considered human tissue at very high frequencies such as 2.4 GHz [9–11]. However, few studies have considered low band frequency and used only one type of biological tissue such as wet skin or dry skin [12, 13].

The main reason for the power dissipation is the implanted coil. Therefore, the coil shape and geometry should be effective and as small as possible with the lowest power dissipation feasible. To address

the above issue, the design and optimization of efficient inductive power links have been well studied in [14]. A spiral rectangular coil implant with dimensions of 25×10 mm and an operating frequency of 13.56 MHz is designed and tested; however, the size of the implanted coil and the short-range coupling are still issues [15]. Another coil with a spiral square shape is designed with dimensions 20 mm $\times$ 8 mm and 1–5 MHz of operating frequency. This coil has performed as an optimum communicating device for 10 mm in distance, but still suffered relatively large size and short-range transmission [12].

Xiuhan et al. [16] designed an implanted circular coil with dimensions of $d_{out} = 18$ mm and $d_{in} = 16$ mm to offer 15 mm of distance coupling with an operating frequency of 742 kHz. However, the large area of the outer diameter is the major drawback of this design [16]. Printed spiral circular coils (PSCCs) are widely used in biomedical application due to their possibility of reducing the coils misalignments for implantation under the skin. The benefits of PSCC are that it can be located inside the human body in a range of depth around 1 mm to 6 mm. Therefore, the PSCCs are suitable for implanted micro-systems and cochlear implants where the depth range is between 2 mm and 6 mm. Moreover, PSCCs can be implanted in 5 mm of depths as in the retinal implants, respectively [17–19]. However, the geometric shape of the coils, their gains, specific absorption rate SAR effect and radiated power loss are still issues for the suitability in the implanted micro-systems.

The issues in the previous introduction motivated us to take care of the dimensions of the new circular spiral coil design process. However, our design aims to perform properly in both wet and dry skin types in a depth of 6 mm. This design is simulated with a commercial field solver ANSOFT-HFSS in the near-field region with a strip line. The SAR effect and power radiation of the coils have been investigated using SEMCAD 14.6 software to claim the suitability of the proposed implanted coils.

2. GEOMETRIC DESIGNS OF SPIRAL CIRCULAR COILS

The circular spiral coil is widely used in inductive coupling link method to power the implanted devices due to its robust application against lateral coil misalignment. Because the external coil is located outside the body, increasing the dimension of the coil does not affect the coil design. However, the implanted coil are limited by many factors such as weight, shape, size and feasibility; hence, the dimension of the internal coil should be as small as possible with the smallest possible

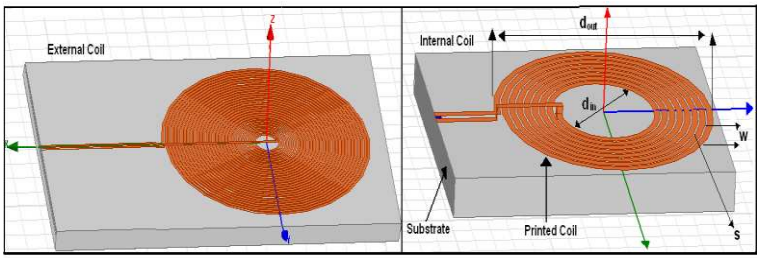

Figure 1. The layout of the spiral circular coils printed on a PCB substrate simulate with HFSS.

number of turns as well as have a low power loss to prevent tissue heating. Both coils are assumed aligned and simulated in the near field as shown in Figure 1. The coils are used for the implanted micro-system applications and radiated in near-field (Fresnel) region at operating frequency 13.56 MHz in narrow-band. The EM fields have omnidirectional radiation, which allows better links with the implanted coil). However, in case of small circular loops, the outer external coil dimensions satisfy the condition given in (1) [20].

$$d_{out} \leq D2\sqrt{2} \tag{1}$$

where D represents the maximum distance at which the coil can radiate and transfer energy. The mutual distance between the transmitter and receiver coils should satisfy the condition given in [21] which we modify in (2)

$$\frac{d_{out\cdot T}}{2} = \sqrt{Z^2 + \frac{d_{out\cdot R}}{2}} \tag{2}$$

where Z represents the mutual distance between coils, and $d_{out\cdot T}$ and $d_{out\cdot R}$ represent the external and internal outer dimensions for the transmitter and receiver coils.

In order to design effective inductive coupling links based on circular spiral coils acting as a transmitter and receiver, the mutual inductance between the coils and the self-inductance of a spiral circular coil with turns should be introduced.

To estimate the mutual inductance of coils, the mutual inductance of two aligned and parallel circular filaments (i.e., single-turn coils) with diameters d_T and d_R, respectively, which are adopted from [22] as illustrated in (3), is assumed.

$$M = \frac{1}{2}\mu_0\sqrt{d_T \times d_R}\left[\left(\frac{2}{f} - f\right)K(f) - \frac{2}{f}E(f)\right] \tag{3}$$

$$f(d_T, d_R, Z) = \left(\frac{4 d_T d_R}{(d_T + d_R)^2 + Z^2} \right)^{\frac{1}{2}} \tag{4}$$

$\mu_o = 4\pi \times 10^{-9}$ H/cm represents the permeability of the free space, and K and E are the complete elliptic integrals of the first and second kind [22]. The total mutual inductance between two coils is calculated by adding the partial mutual inductances between every two turns on a printed spiral coil pair, therefore, will be as follows.

$$M_{ij} = G \sum_{i=1}^{n_1} \sum_{j=1}^{n_2} M_{ij} \left(d_{T \cdot i}, d_{R \cdot j}, Z \right) \tag{5}$$

where M_{ij} is the mutual inductance between loop i of the external coil and loop j of the internal coil, and G presents the factor dependent on the printed spiral shapes, where $G = 1.0$ for the circular shape [23]. The number of turns of the external coil is 30 with separated space of 0.3 mm, and that of the implanted coil is 8 with separated space of 0.1 mm. As the turn spaces are very small, Lyles method [24] is used to consider each external and internal coil having two circular filaments with dimensions $d_{out \cdot T}$, $d_{in \cdot T}$ and $d_{out \cdot R}$, $d_{in \cdot R}$, respectively. Hence, the approximated mutual inductance between two spiral circular coils is found as a function on number of turns for each coil, distance and mutual inductance for the transmit and received filaments coils as given in (6).

$$M(d_T, d_R, Z) \cong N_T N_R \left(\frac{M_{d_{out \cdot T}} + M_{d_{in \cdot T}} + M_{d_{out \cdot R}} + M_{d_{in \cdot R}}}{4} \right) \tag{6}$$

Regarding (3), (4) and (6) the mutual inductance $M_{T \cdot R}$ between pair spiral circular coils, where $d_{out \cdot T} \geq d_{out \cdot R}$, can be simplified, and only the final equations have been provided as given in (7).

$$M_{T \cdot R} \cong \frac{\mu_0 N_T d_{out \cdot T}^2 N_R d_{out \cdot R}^2 \pi}{2\sqrt{\left(d_{out \cdot R}^2 + Z^2 \right)^2}} \tag{7}$$

where N_T and N_R represent the numbers of turns of the transmitter and receiver coils.

To compute the self-inductance of each spiral circular coil, the arithmetic geometrical averages for the external and internal coils should be calculated as given in (8)

$$d_{avg \cdot T} = 0.5 \times \left(d_{out \cdot T} + d_{in \cdot T} \right), \quad d_{avg \cdot R} = 0.5 \times \left(d_{out \cdot R} + d_{in \cdot R} \right) \tag{8}$$

The fill ratio factor φ is a parameter, which changes from 0, when all the turns are concentrated on the perimeter, such as filament coils, and

change to 1, when the turns spiral all the way to the center of the coil. The fill factor for each coil should be calculated as given in (9).

$$\varphi_T = \frac{(d_{out\cdot T} - d_{in\cdot T})}{(d_{out\cdot T} + d_{in\cdot T})}, \quad \varphi_R = \frac{(d_{out\cdot R} - d_{in\cdot R})}{(d_{out\cdot R} + d_{in\cdot R})} \tag{9}$$

The self-inductance of a spiral circular coil is calculated as a semi-empirical and expressed based on equivalent current densities on both sides' spirals. There are many proposed expressions such as Wheeler's expression and optimal expressions [25]. The particular expression used here is selected due to its simplicity and accuracy and gives a result within 5% of the field solver (Fast-Henery 2) or any other field solver used for the same purpose [26]. However, in this design, a particular expression is used due to its simplicity and accuracy as follows.

$$L = \frac{C_1 \mu_0 N^2 d_{avg}}{2} \left[l_n \left(\frac{C_2}{\varphi} \right) + C_3 \varphi + C_4 \varphi^2 \right] \tag{10}$$

where N represents the number of turns, and C is the coefficient on the circular coil layout in terms of values selected as $C_1 = 1.00$, $C_2 = 2.46$, $C_3 = 0.00$, $C_4 = 0.20$ which are adopted from [27]. The accuracy of the designed expression depends on the values of φ and n. The accuracy also depends on the indirect relation of S/W ratio, where S represents the distance between each turn and W the copper line width.

The transmitted and received (implanted coil) pancake coils coupling can be optimized by making $d_{in\cdot T} \approx 0.18 d_{out\cdot T}$ and $d_{in\cdot R} \approx 0.75 d_{out\cdot R}$, respectively, which is adopted from [25]. The commercial field solver ANSOFT-HFSS 13.0 based on the finite-element method (FEM) technique [28] was used to design the proposed coils dimensions

Table 1. The parameter values of the external and internal coils.

Quantity	Symbol	External Coil	Internal Coil
Outer diameter	d_{out}	56 mm	11.6 mm
Inner diameter	d_{in}	10 mm	0.5 mm
Average diameter	d_{avrg}	33 mm	8.25 mm
Inductance	L	4.92 µH	1 µH
Number of turns	N	30	8
Inductor Width	w	0.5 mm	0.3 mm
Turn spacing	S	0.3 mm	0.1 mm

in which $d_{out\cdot T} = 56\,\text{mm}$, $d_{in\cdot T} = 10\,\text{mm}$, and $d_{out\cdot R} = 11.6\,\text{mm}$, $d_{in\cdot R} = 5\,\text{mm}$, respectively. Hence, the external coil is closer to the optimum design by approximately 99%, whereas, the internal coil is closer to the optimum design by 60%. Inserting the above dimensions in Eq. (2), the distance between the two coils is 22 mm. The above geometric design of the spiral circular coil parameter optimization is shown in Figure 2. The designed parameters of external and internal coil dimensions, spacing, operating frequency and related distance are given in Table 1. Both coils are printed on board circuits based on Rogers 4350$^{\text{TM}}$ substrate with constitutive parameters of 1.5 mm substrate thickness, 4.4 (FR4) dielectric constant, 3.66 relative permittivity, 0.004 dielectric loss tangent and "1" relative permeability, respectively.

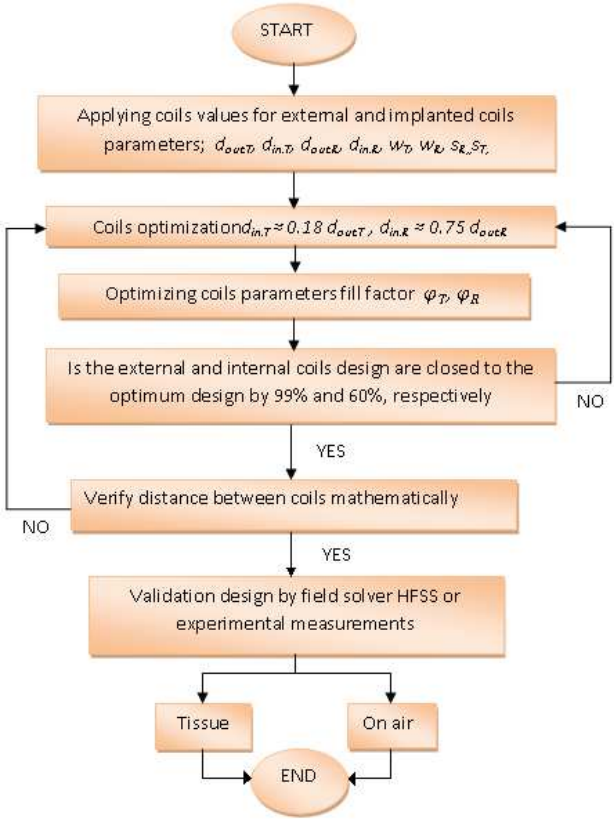

Figure 2. The iterative flowchart optimization coil parameters.

3. MODEL OF HUMAN BIOLOGICAL TISSUE AT 13.56 MHz

As shown in Table 2, the conductivity, permeability and loss-tangent of the human tissue are considered in this design, while the other designers did not consider such constitutive parameters for all tissue layers in their designs as given in literature review [9–13]. They claimed that the frequencies below 20 MHz would have no influence on the tissue. As the external coil contacts the skin, the external magnetic flux links the implanted coil and transfers power through tissue to the implant coil. Our aim is to design a coil compatible with the implanted micro-system for a maximum depth of 6 mm. However, this 6 mm of depth represents 1 mm of skin and 2 mm of fat followed by 3 mm of muscle, where the model occupies $70 \times 60 \times 6$ mm as a dimension as shown in Figure 3.

The tissue model involves two types: the dry skin followed by fat then muscle, and the second type is the wet-skin followed by fat and muscle. These two types have different conductive parameters as given in Table 2 and undergone a test in the near-field, where the electromagnetic fields have been solved for 13.56 MHz using HFSS.

Table 2. The constitutive parameters of the human biological tissue at 13.56 MHz.

Model	Conductivity [Sm^{-1}]	Relative Permittivity	Loss Tangent	Wavelength [m]
Air	0	1	0	22.123
Muscle	0.62818	138.44	6.0152	0.99744
Fat	0.030354	11.827	3.4021	4.264
Dry Skin	0.23802	285.25	1.1062	1.1729
Wet Skin	0.38421	177.13	2.8754	1.1682

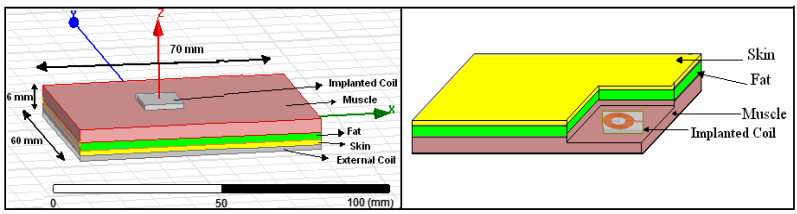

Figure 3. Human biological tissue model dimensions with implanted circular coils in HFSS.

Thus, according to our design, the magnetic region surrounding the implanted coil has occupied a radius of 12.16 µm. Hence, the setting of the sphere radius in HFSS software should be lower than 12.16 µm and selected at 6 µm in order to reach the required near field dimensions. An air box with dimensions of $70 \times 60 \times 55$ mm is determined using the algorithm of the FEM as the radiation boundary.

4. SPECIFIC ABSORPTION RATE (SAR) EFFECT

One of the important situations of transferring signals via inductive coupling is when the tissue faces an electromagnetic field. Such a tissue will derive the power to be dissipated inside the tissue itself. Therefore, the temperature will be increased around the tissue. As a result, the tissues surrounding the coil may be damaged. However, power dissipation should be in the accepted range defined by the international standards of the electromagnetic safety, where these standards meet the limitations of the power dissipation according to the SAR, and calculated as follows [29].

$$\mathrm{SAR} = \frac{d}{dt}\left(\frac{dW}{\rho \times dV}\right) = \frac{\sigma |E|^2}{\rho} \tag{11}$$

In the last expression, dW stands for the time derivative of the energy and dV the incremental mass. The mass density ρ is in kg m^{-3}, conductivity σ in s/m, and finally the r.m.s. amplitude, E, of the electric field is measured in Vm^{-1}. Hence, at a dummy position inside the body, the dissipated power for each unit mass of the tissue will be measured by W kg^{-1}. The sinusoidal excitation can produce a SAR that can be represented mathematically as

$$\mathrm{SAR}(x, y, z) = \frac{\sigma(x, y, z) E^2(x, y, z)}{2\rho(x, y, z)} \tag{12}$$

where x, y, z represent the coordinates of the excited tissue.

Determining SAR is achieved by using numerical techniques or experimental method with fabricated tissue phantoms [30]. In this study, the high accuracy field solver SEMCAD 14.6 is used to determine the SAR using numerical techniques with a finite-difference time domain (FDTD) [31]. The International Commission on Non-Ionizing Radiation Protection (ICNIRP) and Federal Communications Commission (FCC) standards are used in the proposed design [32]. The FCC requires that SAR level at or below 1.6 W kg^{-1} spreads over a volume of 1 g of tissue, whereas the SAR limit is 2 W kg^{-1} averaged over 10 g of tissue. The tissue depth is the depth at which the electric

field has been attenuated by a factor of e^{-1}. This is often calculated as given in (13) which is valid for good material.

$$\delta = \sqrt{\frac{2}{\omega\mu\sigma_e}} \tag{13}$$

where ω is the angular frequency, σ the conductivity of the material, and μ the relative permeability. The tissue depth is defined by calculating the attenuation as $e^{-\alpha z}$ where α represents the attenuation constant and calculated as given in (14) where ε represents the permittivity.

$$\alpha = \omega\sqrt{\frac{\mu\varepsilon}{2}}\left[\sqrt{1+\left(\frac{\sigma}{\omega\varepsilon}\right)^2}-1\right] \tag{14}$$

where

$$\delta = \frac{1}{\alpha} \tag{15}$$

The biological tissue acts as the medium, which is separated between the coils. Thus, the SAR and power losses of the proposed coils operated at 13.56 MHz would not damage the tissue. To prove that, the implanted coil is designed using Pspice compatible with the SEMCAD and powered with 5 voltages and 165 mW. Then the implanted coil inserted at two positions of each at a depth of less than 1 cm. One position is the top of the head in the space between the skull and brain, and the other is near the humerus voluntary muscle of the left hand. The power loss within the tissue can be calculated as follows.

$$20\log_{10}\left(e^{\alpha z}\right) \tag{16}$$

where z represents the depth or the tissue thickness in the case of the implanted micro system. The power dissipation per unit mass of the tissue at any point of the human body is expressed in watts per kilogram. Therefore, the power loss in decibels needs to be converted into watts. Thus, power loss is calculated in terms of the power of the conductivity loss $P_{\sigma loss}$ and radiated power P_{rad} as follows.

$$P_{loss} = P_{\sigma loss} + P_{rad} \tag{17}$$

This calculated SAR using simulation at coordinates (x, y, z, f_o) in our chosen positions and power loss in the tissue will be compared with the standards SAR and power loss data to justify the efficiency of the developed system.

5. RESULTS AND DISCUSSIONS

One of the main drawbacks and challenges of the WPT method is low efficiency due to weak coupling. To overcome this disadvantage, many

issues need to be considered such as coil design. The performance of the proposed coils in air and in human biological tissue is designed, analyzed and optimized using commercial field solver ANSOFT-HFSS 13.0 based on FEM. The results are plotted and analyzed to explain he coil's performance in the near-field, which involves many resultant plots, such as max near field which presents the maximum radiated electric field in the near region, and near E total which is calculated by the combined magnitude of the electric field components such as Near E phi, Near E Theta, etc. Table 3 shows the performance of the external and internal coils based on the gain, angle drop of the plane and the radiated power efficiency in the air, wet skin, and dry skin, respectively. The results show that the maximum gains for the external coil are in air 54 dB, in wet-skin tissue 49.80 dB, and dry-skin tissue 48.95, respectively. The maximum gain for the internal coil is in air 53.30 dB, wet skin 41.80 dB and dry skin 41.40 dB, respectively. The external and internal coil radiation efficiencies in wet skin are 92% and 78.4%, whereas, the radiation efficiencies in dry skin are 90% and 77.6%, respectively.

Table 3. Spiral pancake coils performance on air and within dry and wet skin.

Features	External Coil			Internal Coil		
	On Air	Wet skin	Dry skin	On Air	Wet skin	Dry skin
Max. Gain dB	54	49.80	48.95	53.30	41.80	41.40
Total θ Gain dB	47.10	49.80	48.95	53.30	26.60	26.60
Total Φ Gain dB	54	49.70	48.90	53.30	41.70	41.70
Angle Drop at θ Plane	140° and 325°	270°	275° and 320°	10° and 220°	310°	85° and 285°
Radiation Efficiency	—	92%	90%	—	78.4%	77.6%

In order to clarify the results to be understandable, the external coil performance is first plotted on air with a relative distance 6 mm. Then the coil is attached to the tissue that involves wet skin and dry skin with a thickness of 6 mm. Figure 4 shows the 2D radiation patterns of total and max near-field in the external coil on air, the maximum

and total near-field on the elevation plan at $\Phi = 90°$ and $\Phi = 0°$ is 54 dB. The total near gain on the azimuthal plan $\theta = 90°$ and $\theta = 0°$ is 47.10 dB and approximately 47 dB, respectively. There is a very slight drop on the azimuthal plane $\theta = 90°$ at angles 140° and 325°.

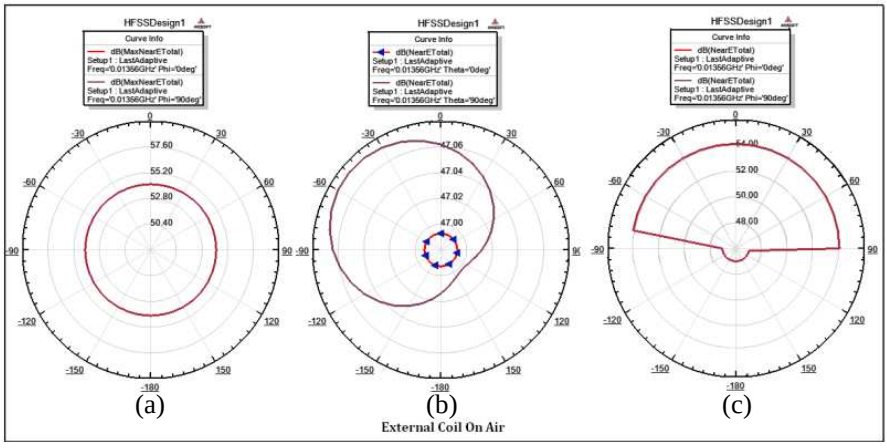

Figure 4. Simulated radiation patterns for the external coil on air: (a) max gain on planes ($\Phi = 0°$, $\Phi = 90°$), (b) on the azimuthal plane ($\theta = 0°$, $\theta = 90°$), and (c) on the elevation plane ($\Phi = 0°$, $\Phi = 90°$), respectively.

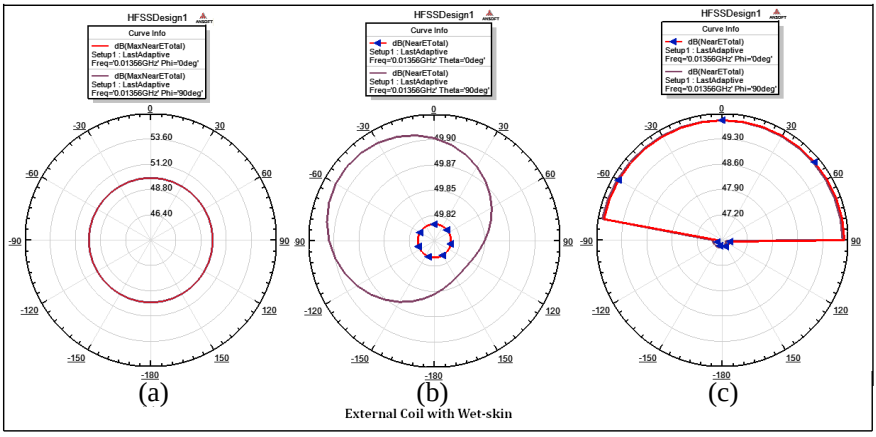

Figure 5. Simulated radiation patterns for the external coil inside a wet skin: (a) max gain on planes ($\Phi = 0°$, $\Phi = 90°$), (b) on the azimuthal plane ($\theta = 0°$, $\theta = 90°$), and (c) on the elevation plane ($\Phi = 0°$, $\Phi = 90°$), respectively.

Figures 5 and 6 show the 2D of the external coil radiation gain when the coil is attached to the tissue that involves wet and dry skins, respectively. Figure 7 shows slight drops in some specific angles. The results show that the maximum and total gain inside a wet skin on elevation ($\Phi = 90°$, $\Phi = 0°$) and azimuthal plans ($\theta = 90°$, $\theta = 0°$) is approximately 49.80 dB. The maximum and total gain inside a dry skin in elevation and azimuthal plans is approximately 48.95 dB, and there is a very slight drop on the azimuthal plane inside the wet skin at angle 270° and inside the dry skin at angles 275° and 320°, respectively. The results above show that the external coil has a very

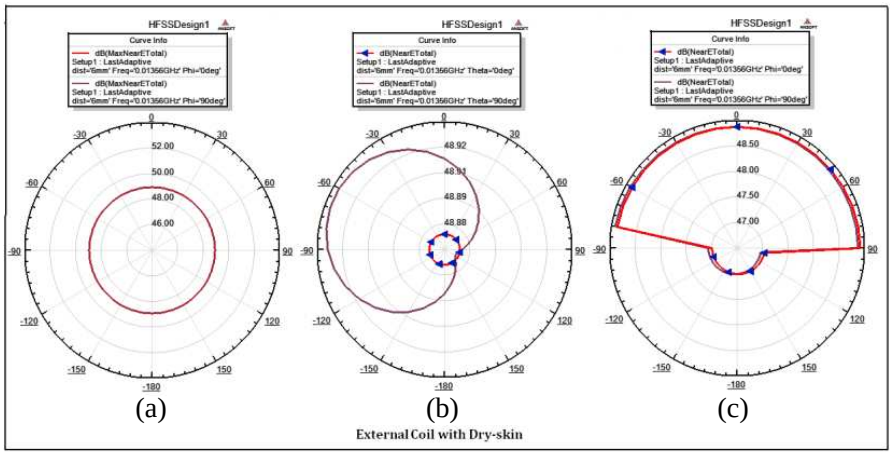

Figure 6. Simulated radiation patterns for the external coil inside a dry skin: (a) max gain on planes ($\Phi = 0°$, $\Phi = 90°$), (b) on the azimuthal plane ($\theta = 0°$, $\theta = 90°$), and (c) on the elevation plane ($\Phi = 0°$, $\Phi = 90°$), respectively.

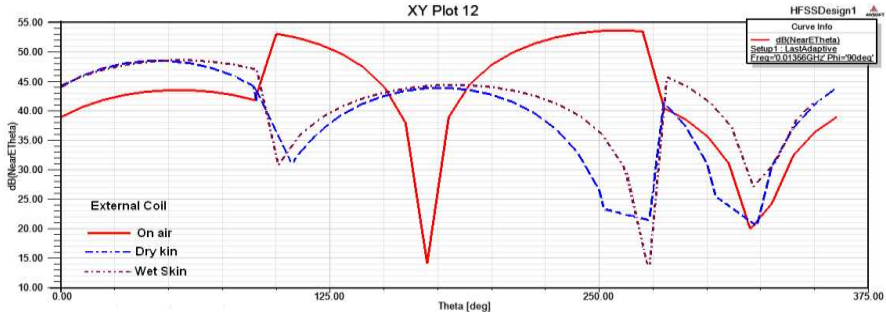

Figure 7. Slight drop in radiation for the external coil.

stable omnidirectional radiation, and the coil performance within tissue is reduced only approximately 9% than that on air. The dry skin results in reduced gain only 1 dB less than in wet skin. Thus, the skin condition does not affect the efficiency of the coil performance.

Figure 8 shows the 2D radiation patterns of the internal coil on air. The maximum and total gain in the near field on the azimuthal plane ($\theta = 90°$, $\theta = 0°$) and the elevation plane ($\Phi = 90°$, $\Phi = 0°$) is 53.30 dB. There is a very slight drop at angles 10° and 220° on the azimuthal plane ($\theta = 90°$), and the radiation is omnidirectional.

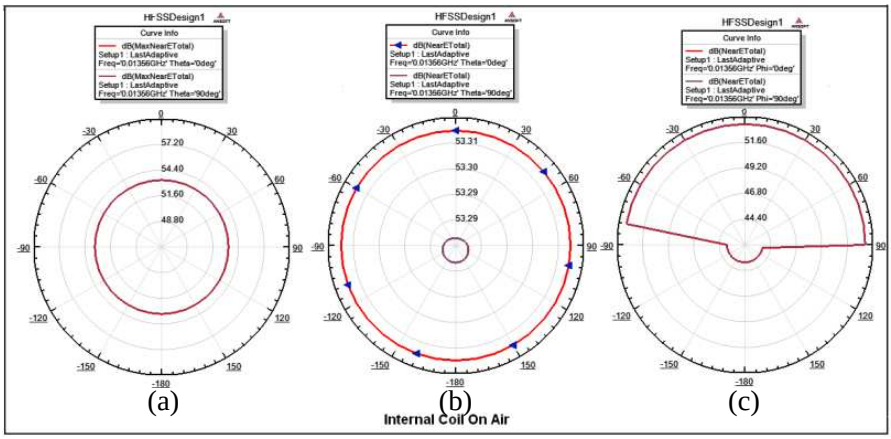

Figure 8. Simulated radiation patterns for the internal coil on air: (a) max gain on planes ($\Phi = 0°$, $\Phi = 90°$), (b) on the azimuthal plane ($\theta = 0°$, $\theta = 90°$), and (c) on the elevation plane ($\Phi = 0°$, $\Phi = 90°$), respectively.

Figures 9 and 10 show the 2D radiation gain of the internal coil when it is mounted with depth 6 mm in the tissue involving wet and dry skin, respectively. Figure 11 shows a slight drops in some specific angles. The results show that the maximum gain with wet skin of the elevation plane ($\Phi = 90°$, $\Phi = 0°$) is 41.80 dB. The total gains on the azimuthal plane ($\theta = 90°$, $\theta = 0°$) and elevation plane ($\Phi = 90°$, $\Phi = 0°$) are approximately from 25.30 dB to 26.60 dB and 41.70 dB, respectively, and there is a drop on the azimuthal plane at the angle 310° when $\theta = 90°$. The maximum gain for the dry skin is 41.40 dB, and the same results are found in total gain inside both wet and dry skins. There is a slight drop on the azimuthal plane at angles 85° and 285°, respectively. The above results show that the internal coil has a stable omnidirectional radiation on air, and the coil performance within tissue at depth 6 mm is reduced approximately

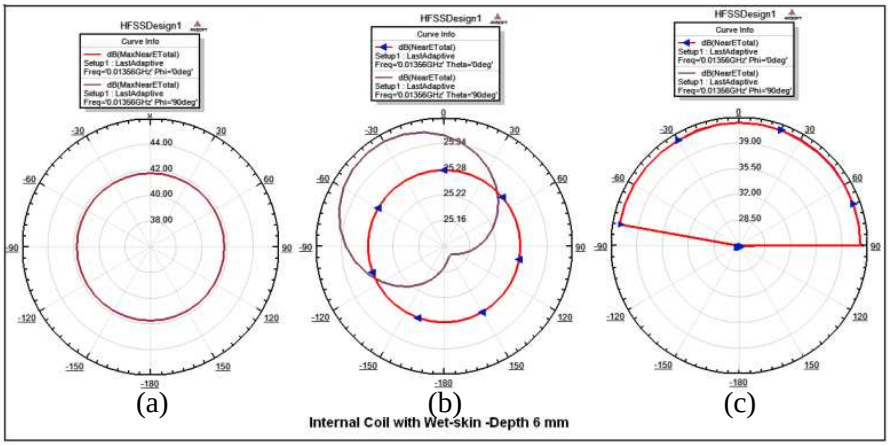

Figure 9. Simulated radiation patterns for the internal coil inside a wet skin: (a) max gain on planes ($\Phi = 0°$, $\Phi = 90°$), (b) on the azimuthal plane ($\theta = 0°$, $\theta = 90°$), and (c) on the elevation plane ($\Phi = 0°$, $\Phi = 90°$), respectively.

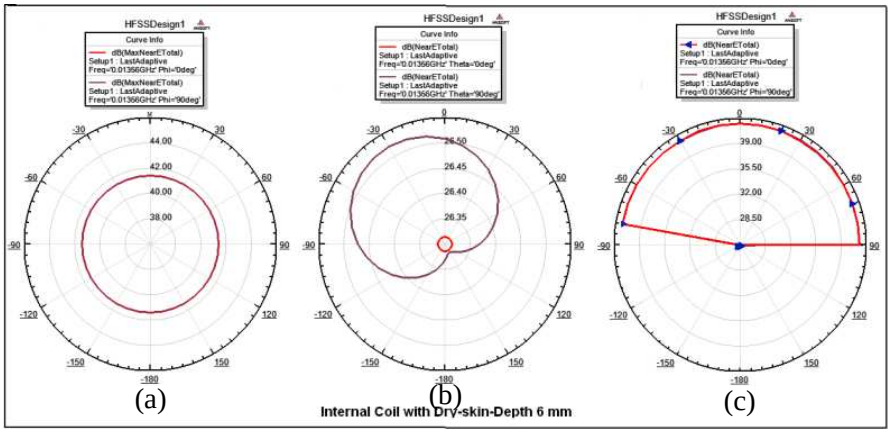

Figure 10. Simulated radiation patterns for the internal coil inside a dry skin: (a) max gain on planes ($\Phi = 0°$, $\Phi = 90°$), (b) on the azimuthal plane ($\theta = 0°$, $\theta = 90°$), and (c) on the elevation plane ($\Phi = 0°$, $\Phi = 90°$), respectively.

21% due to tissue attenuations.

Based on the above results and figures, the external coil on the azimuthal plane ($\theta = 90°$, $\theta = 0°$) and elevation plane ($\Phi = 90°$, $\Phi = 0°$) have approximately the same radiation gain and an omnidirectional

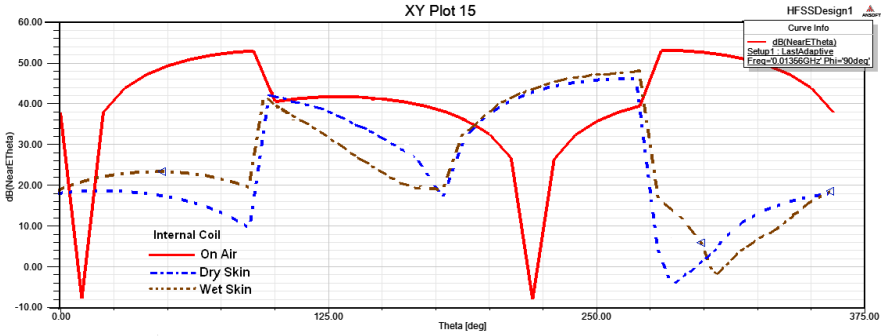

Figure 11. Slight drop in radiation for the internal coil.

radiation at all angles, except that there is a very slight drop in some specific angles in theta view which does not affect the coil's performance.

To verify implanted coil design, Table 4 shows the comparison between the proposed design and other works. The proposed design has smaller size and longer operational distance.

Table 4. Comparison between proposed design and other works.

References	[12]	[15]	[16]	Proposed
Shape of Coil	Spiral Square	Spiral Rectang	Circular	Spiral Circular
Frequency	1–5 MHz	13.56 MHz	742 KHz	13.56 MHz
Dimension	20 mm × 8 mm	25 mm × 10 mm	$d_{out} = 18$ mm $d_{in} = 16$ mm	$d_{out} = 11.6$ mm $d_{in} = 5$ mm
Distance	10 mm	10 mm	15 mm	22 mm

The implanted coil is a receiving mode system; hence, it is very important to calculate the SAR and radiated power for the implanted coil. Before calculating SAR and power loss, the implanted coil performance should be investigated on air and within simulated biological human tissues. The software SEMCAD 14.6 is used to validate and determine the SAR, power loss and energy density that occurs because of transmitted EM signal and implanted coil power radiated. In order to prove that the radiated power of the implanted coil does not damage the biological human tissue, we inserted the implanted coil inside the human tissues at two positions with 1 cm of depth. The coil is powered with 5 V, 165 mW from the external coil. The two points chosen are the muscle of the left hand and between the

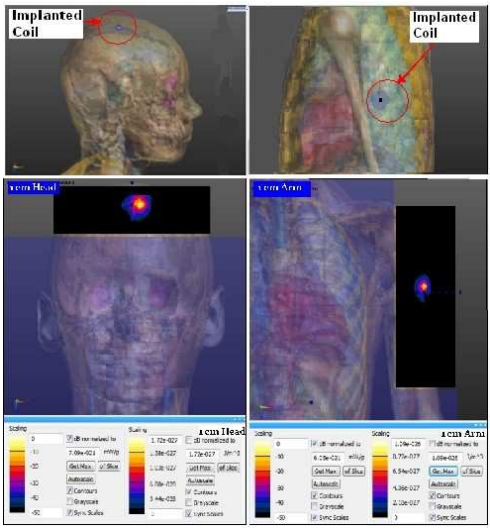

Figure 12. SAR and power loss effects on human tissue at 13.56 MHz.

skull and brain as shown in Figure 12.

The results for the two positions given in Figure 12 are as follows. SAR (x, y, z, f_0) is (2.43×10^{-16} mWg^{-1}) and (6.05×10^{-21} mWg^{-1}), respectively. Energy density (x, y, z, f_0) is (1.09×10^{-26} Jm^{-3}) and (1.72×10^{-26} Jm^{-3}), respectively. Power loss is (1.402×10^{-25} W) and (1.8364×10^{-25} W), respectively. The above results show that the SAR is much less than the standard for 1 g and negligible for 10 g and that the power loss effect is negligible. Namely, the proposed implanted coil has negligible SAR and power loss effect.

6. CONCLUSION

In this study, an inductive link based on spiral circular (pancake) design is developed and tested on air and within the biological human tissue at frequency 13.56 MHz. The proposed coupling coils are suitable for the use in implanted micro-systems, cochlear implants. The commercial HFSS software was used to design and simulated the proposed coils, and the coil geometries are given in Table 1. To study the coil's performance, the behavior of the coil is simulated in air and in proposed human biological tissue models including dry or wet skin using constitutive parameters at 13.56 MHz. The implanted coil is mounted inside the tissue at a depth up to 6 mm. The effect of the skin condition (dry or wet) is very small and can be ignored. The

specific absorption rate (SAR) and the power loss are extremely small, thus, leading to a not increasing tissue temperature and not damaged. Finally, the proposed implanted coil is small and performs well, making it highly suitable for being implanted in micro-systems.

ACKNOWLEDGMENT

This work was supported by the Universiti Kebangsaan Malaysia under Grant UKM-DLP-2012-002.

REFERENCES

1. Hannan, M., M. Saad, A. S. Salina, and H. Aini, "Modulation techniques for biomedical implanted devices and their challenges," *Sensor*, Vol. 12, 297–319, 2012.
2. Wang, G., W. Liu, M. Sivaprakasam, and G. Alperkendir, "Design and analysis of an adaptive transcutaneous power telemetry for biomedical implants," *IEEE Trans. Circuits and Syst. I*, Vol. 52, 2109–2117, 2005.
3. Lee, S. B., H. M. Lee, M. Kiani, U. Jow, and M. Ghovanlo, "An inductively powered scalable 32-channel wireless neural recording system on achip for neuroscience applications," *IEEE Trans. Biomed. Circuits and Systems*, Vol. 4, 360–371, 2010.
4. Saad, M., M. A. Hannan, A. Salina, and A. Hussain, "Efficient data and power transfer for bio-implanted devices based on ASK modulation techniques," *J. of Mech. in Medi. and Biology.*, Vol. 12, 1–17, 2012.
5. Chih, K. L., J. C. Jia, L. C. Cho, L. C. Chen, and W. Chua, "An implantable bi-directional wireless transmission system for transcutaneous biological signal recording," *Physiol. Meas.*, Vol. 26, 83–97, 2005.
6. Park, S. I., "Enhancement of wireless power transmission into biological tissue using a high surface impedance ground plane," *Progress In Electromagnetics Research*, Vol. 135, 123–136, 2013.
7. Gabriel, C., S. Gabriely, and E. Corthout, "The dielectric properties of biological tissues: I, II and III, literature survey," *J. of Phys. Med. Biol.*, Vol. 41, 2231–2293, 1996.
8. Lin, J. C., "Computer methods for field intensity predictions," *CRC Handbook of Biological Effects of Electromagnetic Fields*, C. Polk and E. Postow, Eds., Vol. 22, 73–313, CRC Press, Boca Raton, FL, 1986.

9. Karacolak, T., R. Cooper, and E. Topsakal, "Electrical properties of rat skin and design of implantable antennas for medical wireless telemetry," *IEEE Trans. on Antennas and Propagation*, Vol. 57, 2806–2812, 2009.
10. Al Shaheen, A., "New patch antenna for ISM band at 2.45 GHz," *ARPN. J. of Eng. and Applied Sciences*, Vol. 7, 1–9, 2012.
11. Zhu, F., S. Gao, A. T. S. Ho, C. H. See, R. A. Abd-Alhameed, J. Li, and J.-D. Xu, "Design and analysis of planar ultra-wide and antenna with dual-notched function," *Progress In Electromagnetics Research*, Vol. 127, 523–536, 2012.
12. Meysam, Z. and P. G. Gulak, "Maximum achievable efficiency in nearfield coupled power-transfer systems," *IEEE Trans. Biomed. Circuits and Systems*, Vol. 6, 228–245, 2012.
13. Uei, M. J. and M. Ghovanloo, "Modeling and optimization of printed spiral coils in air and muscle tissue environments," *IEEE 31st Annual International Conference of the (EMBS)*, 6387–6390, Minneapolis, Minnesota, USA, Sep. 2–6, 2009.
14. Zeng, F. G., S. Rebscher, W. Harrison, X. Sun, and H. Feng, "Cochlear implants: System design, integration, and evaluation," *IEEE Rev. Biomed. Eng.*, Vol. 1, 115–142, 2008.
15. Luis, A., F. X. Rui, W. C. Kuang, and J. Minkyu, "Closed loop wireless power transmission for implantable medical devices," *IEEE 13th International Conference on Integrated Circuits*, 404–407, Singapore, Dec. 12–14, 2011.
16. Li, X., H. Zhang, F. Peng, Y. Li, T. Yang, B. Wang, and D. Fang, "A wireless magnetic resonance energy transfer system for micro implantable medical sensors," *Sensors*, Vol. 12, 10292–10308, 2012.
17. Harrison, R. R., P. T. Watkins, R. J. Kier, R. O. Lovejoy, D. J. Black, B. Greger, and F. Solzbacher, "A low-power integrated circuit for a wireless 100-electrode neural recording system," *IEEE J. Solid-State Circuits*, Vol. 42, 123–133, 2007.
18. Clark, G. M., *Cochlear Implants: Fundamentals and Applications*, Ch. 8, Springer-Verlag, New York, 2003.
19. Humayun, M. S., J. D. Weiland, G. Y. Fujii, R. Greenberg, R. Williamson, J. Little, B. Mech, V. Cimmarusti, G. V. Boemel, G. Dagnelie, and E. Juan, "Visual perception in a blind subject with a chronic microelectronic retinal prosthesis," *Vis. Res.*, Vol. 43, 2573–2581, 2003.
20. Finkenzeller, K., *RFID Handbook: Fundamentals and Applications in Contactless Smart Cards and Identification*, 2nd Edition,

Wiley, New York, 2003.

21. Ko, W. H., S. P. Liang, and C. D. Fung, "Design of radio-frequency powered coil for implanted instruments," *Journal of Med. Bio. Eng. Compute.*, Vol. 15, 634–640, 1977.
22. Mohan, S., D. C. Galbraith, and R. L. White, "Radio-frequency coils in implantable devices: Misalignment analysis and design procedure," *IEEE Trans. Biomed. Eng.*, Vol. 34, 276–282, 1987.
23. Uei, M. J. and G. Maysam, "Design and optimization of printed spiral coils for efficient transcutaneous inductive power transmission," *IEEE Trans. Biomed. Circuits and Systems*, Vol. 1, No. 3, 193–202, 2007.
24. Grover, F. W., *Inductance Calculations: Working Formulas and Tables*, D. Van Nostrand Co., New York, 1946.
25. Harrison, R. R., "Designing efficient inductive power links for implantable devices," *IEEE International Conference on Circuits and Systems*, 2080–2083, New Orleans, USA, May 27–30, 2007.
26. Silay, K. M., C. Dehollaini, and M. Declercq, "Improvement of power efficiency of inductive links for implantable devices," *IEEE Conference on Research in Microelectronics and Electronics*, 229–232, Istanbul, Turkey, Apr. 22–25, 2008.
27. Mohan, S., M. Hershenson, S. P. Boyd, and T. H. Lee, "Simple accurate expressions for planar spiral inductances," *IEEE J. Solid-State Circuits*, Vol. 34, 1419–1424, 1999.
28. Felippa, C. A., "Introduction to finite element method," available online at http://caswww.colorado.edu/courses.d/IFEM.d/IFEM.Ch01.d/IFEM.Ch01.pdf.
29. IEEE C95.1-2005, "IEEE standards for safety levels with respect to human exposure to radio frequency electromagnetic fields, 3 kHz to 300 GHz," Institute of Electrical and Electronics Engineers, New York, 2005.
30. Lazzi, G., "Power dissipation characteristics and computational methods," *IEEE Journal of Engineering in Medicine and Biology Magazine*, 75–81, 2005.
31. Fujimoto, M., A. Hirata, J. Wang, O. Fujiwara, and T. Shiozawa, "FDTD-derived correlation of maximum temperature increase and peak SAR in child and adult head models due to dipole antenna," *IEEE Trans. on Electromagnetic Compatibility*, Vol. 48, No. 1, 240–247. Feb. 2006.
32. Office of Engineering Technology, "Understanding the FCC regulations for low-power, non-licensed transmitters," OET Bulletin No. 63, Oct. 1993.